Resources, Conservation & Recycling 143 (2019) 167–177

Contents lists available at ScienceDirect

Resources, Conservation & Recycling

journal homepage: www.elsevier.com/locate/resconrec

Full length article

Source contributions to poor atmospheric visibility in China

Xun Li[a], Lin Huang[a], Jingyi Li[a], Zhihao Shi[a], Yiyi Wang[a], Hongliang Zhang[b], Qi Ying[c], Xingna Yu[d], Hong Liao[a], Jianlin Hu[a,*]

[a] Collaborative Innovation Center of Atmospheric Environment and Equipment Technology, Jiangsu Key Laboratory of Atmospheric Environment Monitoring and Pollution Control, Nanjing University of Information Science & Technology, Nanjing 210044, China
[b] Department of Civil and Environmental Engineering, Louisiana State University, Baton Rouge, LA, 70803, USA
[c] Zachry Department of Civil Engineering, Texas A&M University, College Station, TX, 77843, USA
[d] Key Laboratory of Meteorological Disaster-Ministry of Education, Joint International Research Laboratory of Climate and Environment Change, Collaborative Innovation Center on Forecast and Evaluation of Meteorological Disasters, Key Laboratory for Aerosol-Cloud-Precipitation of China Meteorological Administration, Nanjing University of Information Science and Technology, 210044, China

ARTICLE INFO

Keywords:
Source apportionment
Light extinction coefficient
Source-oriented model
Visibility impairment
China

ABSTRACT

China suffers from serious haze pollution characterized by extremely low visibility due to intensive air pollutant emissions. Designing effective visibility impairment control strategies requires quantitative measures of the contributions of different sources. In this study, a source-oriented Community Multiscale Air Quality model was applied to quantitatively determine the source contributions to visibility impairment in China in 2013. Emissions of air pollutants from seven source categories (power plants, residential sources, industries, transportation, open burning, dust, and agriculture) were separately tracked. The industrial sector dominates the visibility impairment in Beijing, Chongqing, Guangzhou, and Shanghai, contributing to 32.6–40.7% of the overall light extinction coefficient (b_{ext}). Agriculture and power sources contribute 13.0–16.7% and 12.6–14.9% to b_{ext}, respectively. The residential sector is the largest source of visibility impairment in Xi'an (39.5%). It also contributes 12.3–25.2% in Beijing, Chongqing, Guangzhou, and Shanghai. Transportation (6.3–10.2%), open burning (1.7–8.8%), and dust emission (1.0–3.6%) have relatively smaller contributions to b_{ext} in these cities. The source contributions to b_{ext} exhibit strong spatial and seasonal variations. Contributions from industrial, power, and residential sectors are higher in the North China Plain, Northeast China, and Sichuan Basin than in other regions of China. Industrial and residential emissions become the most important sources of visibility impairment in winter. In other seasons, industrial, power, and agriculture sources are important. The large spatial and seasonal variations in the sources of b_{ext} suggest that different pollutants mitigation programs should be designed for different regions and times of the year.

1. Introduction

Visibility, an indicator of the atmospheric transparency, refers to the visual range that distant objects can be clearly discerned. Visibility is a very important natural resource and also an important factor for the protection of transportation safety. Visibility in the pristine atmosphere is only influenced by light scattering of gas molecules (i.e., Rayleigh scattering) and can reach approximately 300 km. In contaminated areas, anthropogenic gaseous and particulate pollutants can cause significant visibility impairment by scattering and absorbing light. Light scattering by particles is the main reason for reduced visibility in most areas (Hyslop, 2009).

China suffers from serious haze pollution characterized by extremely low visibility caused by high loadings of fine particulate matter ($PM_{2.5}$). Along with the rapid economic growth and intensive emissions from a large amount of fossil fuel consumption (Zeng et al., 2019; Huang et al., 2017), urban and regional visibility in China has been deteriorating (Chang et al., 2009; Che et al., 2009; Hu et al., 2017c; Li et al., 2016a; Deng et al., 2014; Cheng et al., 2013b). Visibility impairment during haze pollution events has caused serious negative impacts on transportation, economic production, and people's living. Therefore, developing emission control programs to improve visibility in urgently needed in China.

The first step in developing an effective visibility improvement program through emission control is to thoroughly understand the contributions of different sources to visibility impairment. Previous

* Corresponding author.
E-mail address: jianlinhu@nuist.edu.cn (J. Hu).

https://doi.org/10.1016/j.resconrec.2018.12.029
Received 22 September 2018; Received in revised form 26 December 2018; Accepted 26 December 2018

analyses have shown that the most important sources of light absorption are gas-phase NO_2 and particle-phase elemental carbon (Trijonis, 1984), and the main sources of light scattering are associated with ammonium, sulfate, organic carbon and nitrate (Sisler and Malm, 1994). Furthermore, statistical analysis of long-term datasets shows that there is a significant correlation between the visibility and the relative humidity (RH) of ambient air (Deng et al., 2011; Xiao et al., 2011).

A few studies have investigated the source contributions to light extinction in China (Tao et al., 2014; Cao et al., 2012a; Wang et al., 2013) using the receptor-based models. These studies focused on a few megacities, such as Chengdu and Xi'an in China. Due to limitations in the receptor-based models, the source contribution of secondary particulate matter (PM), which generally accounts for a significant fraction of the total $PM_{2.5}$ mass (Huang et al., 2014), was not quantitatively estimated. Source-oriented air quality models were developed to accurately determine source contributions to primary and secondary $PM_{2.5}$. Ying et al. (2004) and Chen et al. (2009) have used source-oriented air quality models to successfully predict source contributions to visibility impairment in the United States.

A source-oriented Community Multiscale Air Quality (CMAQ) modeling system has been developed and applied to predict the concentrations of gaseous and particulate pollutants and their spatial and temporal variations in 2013 in China (Hu et al., 2016, 2017b; Ying et al., 2018), and to quantify the contributions of different source sectors to $PM_{2.5}$ (Hu et al., 2017a; Chen et al., 2019) and its components, including primary $PM_{2.5}$ (Hu et al., 2015b), secondary inorganic $PM_{2.5}$ (i.e., ammonium ion, sulfate, and nitrate) (Shi et al., 2017), and secondary organic $PM_{2.5}$ (Wang et al., 2018). The predicted source contributions to detailed $PM_{2.5}$ components make it possible to further determine the contributions of different source sectors to visibility impairment. The objective of this study is to quantify the source contributions to visibility impairment in 2013 in China using the source-oriented CMAQ model predictions. Model predicted light extinction coefficient (b_{ext}) is evaluated against b_{ext} calculated from observed visual range data. Contributions of different b_{ext} components to the total are estimated. The contributions of different sources to b_{ext} are then quantified using the source apportionment results of the $PM_{2.5}$ components predicted by the source-oriented CMAQ model. The results of this study will improve our understanding of the major sources that affect visibility impairment in China, and provide valuable scientific information for designing effective control strategies to improve visibility.

2. Method

2.1. Source oriented CMAQ model

The source-oriented CMAQ model applied in this study was developed based on CMAQ v5.0.1. The features and algorithms of the source-oriented CMAQ model were described in details by Shi et al. (Shi et al., 2017). A few updates were made to the original CMAQ model, including heterogeneous formation pathways of secondary inorganic (i.e., sulfate and nitrate) and organic aerosols. Details about the updates were documented in previous studies (Hu et al., 2016, 2017b) and references therein. The source-oriented CMAQ model was applied to simulate air quality in China using a 36 × 36 km^2 horizontal resolution for the entire year of 2013. Anthropogenic emissions in China were based on the Multi-resolution Emission Inventory for China of 2012 (MEIC) developed by Tsinghua University (http://www.meicmodel.org), and in other countries were based on the Regional Emission inventory in Asia version 2 (REAS2) (Kurokawa et al., 2013). Biogenic emissions were generated using the Model for Emissions of Gases and Aerosols from Nature (MEGAN) v2.1. Meteorological conditions were simulated using the Weather Research and Forecasting (WRF) v3.6.1. Details of model configurations of the CMAQ, MEGAN, and WRF models and other inputs such as initial conditions and boundary conditions were provided in Hu et al. (2016) and therefore not repeated here.

Model performance on predicting the temporal and spatial variation of air pollutants in China has been extensively evaluated. Hu et al. (2016, 2017b) compared modeled $PM_{2.5}$, O_3, and other criteria pollutants against ambient air quality observations at 422 sites in China, and calculated statistical matrix such as mean fractional bias (MFB), mean

Table 1
Model performance of predicted light extinction coefficients in 59 cities in China. MO: mean observations; MP: mean predictions; MFB: mean fractional bias; MFE: mean fractional errors.

City	first method				second method			
	MO	MP	MFB	MFE	MO	MP	MFB	MFE
Baoding	0.29	0.44	0.11	0.53	0.29	0.64	0.36	0.69
Beijing	0.29	0.31	−0.07	0.41	0.29	0.45	0.17	0.53
Cangzhou	0.28	0.38	0.02	0.49	0.28	0.56	0.31	0.62
Changchun	0.27	0.33	−0.17	0.59	0.27	0.48	0.05	0.7
Changsha	0.24	0.73	0.81	0.84	0.24	1.04	1.02	1.04
Chengde	0.15	0.22	0.07	0.54	0.15	0.31	0.26	0.68
Chengdu	0.3	0.46	0.26	0.44	0.3	0.67	0.55	0.67
Chongqing	0.53	0.56	−0.15	0.46	0.53	0.78	0.13	0.49
Dalian	0.22	0.21	−0.28	0.54	0.22	0.29	−0.07	0.6
Fuzhou	0.2	0.13	−0.51	0.63	0.2	0.16	−0.4	0.63
Guangzhou	0.2	0.24	0.07	0.42	0.2	0.29	0.19	0.48
Guiyang	0.24	0.41	0.1	0.61	0.24	0.55	0.27	0.76
Haerbin	0.23	0.49	0.4	0.66	0.23	0.7	0.64	0.87
Haikou	0.15	0.14	−0.31	0.61	0.15	0.18	−0.24	0.69
Handan	0.39	0.62	0.16	0.44	0.39	0.92	0.49	0.63
Hangzhou	0.55	0.38	−0.32	0.48	0.55	0.56	−0.02	0.43
Hefei	0.41	0.54	0.07	0.44	0.41	0.78	0.36	0.59
Hengshui	0.25	0.47	0.31	0.53	0.25	0.69	0.6	0.74
Huaian	0.61	0.41	−0.44	0.58	0.61	0.59	−0.16	0.53
Huhehaote	0.19	0.2	−0.17	0.63	0.19	0.27	−0.02	0.71
Huzhou	0.44	0.33	−0.36	0.49	0.44	0.46	−0.11	0.48
Jiaxing	0.27	0.3	0.03	0.44	0.27	0.42	0.27	0.6
Jinan	0.24	0.4	0.31	0.52	0.24	0.61	0.6	0.74
Jinhua	0.28	0.17	−0.66	0.73	0.28	0.25	−0.46	0.71
Kunming	0.19	0.18	−0.3	0.65	0.19	0.24	−0.16	0.74
Langfang	0.36	0.41	−0.1	0.5	0.36	0.59	0.18	0.59
Lanzhou	0.21	0.12	−0.66	0.72	0.21	0.16	−0.52	0.72
Lasa	0.1	0.02	−1.32	1.32	0.1	0.02	−1.34	1.34
Lianyungang	0.39	0.34	−0.23	0.52	0.39	0.49	0.02	0.57
Lishui	0.3	0.14	−0.9	0.95	0.3	0.19	−0.75	0.89
Nanchang	0.32	0.29	−0.32	0.49	0.32	0.41	−0.08	0.55
Nanjing	0.37	0.41	−0.04	0.4	0.37	0.61	0.27	0.53
Nanning	0.21	0.25	−0.02	0.45	0.21	0.33	0.13	0.57
Nantong	0.45	0.46	−0.03	0.4	0.45	0.65	0.24	0.5
Qingdao	0.31	0.38	0	0.49	0.31	0.55	0.28	0.62
Qinghuang	0.23	0.4	0.21	0.59	0.23	0.54	0.41	0.73
Quzhou	0.36	0.22	−0.64	0.72	0.36	0.3	−0.45	0.68
Shanghai	0.23	0.31	0.23	0.42	0.23	0.44	0.48	0.6
Shaoxing	0.26	0.22	−0.32	0.5	0.26	0.31	−0.13	0.54
Shenyang	0.23	0.47	0.27	0.63	0.23	0.69	0.49	0.78
Shijiazhuang	0.32	0.42	−0.04	0.52	0.32	0.63	0.24	0.66
Suqian	0.38	0.38	−0.12	0.44	0.38	0.56	0.16	0.53
Suzhou	0.31	0.26	−0.3	0.47	0.31	0.37	−0.04	0.46
Taiyuan	0.24	0.28	0.02	0.38	0.24	0.4	0.26	0.51
Taizhoushi	0.35	0.43	0.09	0.42	0.35	0.62	0.37	0.59
Taizhou	0.3	0.25	−0.2	0.34	0.3	0.37	0.11	0.44
Tangshan	0.3	0.43	0.19	0.45	0.3	0.63	0.48	0.64
Tianjin	0.32	0.4	0.02	0.49	0.32	0.59	0.31	0.61
Wenzhou	0.24	0.13	−0.78	0.85	0.24	0.16	−0.68	0.82
Wuhan	0.28	1.03	0.87	0.91	0.28	1.4	1.08	1.1
Wulumuqi	0.13	0.16	−0.32	0.72	0.13	0.18	−0.28	0.74
Wuxi	0.41	0.31	−0.37	0.47	0.41	0.45	−0.09	0.46
Xian	0.26	0.36	0.05	0.46	0.26	0.52	0.3	0.59
Xining	0.14	0.11	−0.4	0.55	0.14	0.13	−0.31	0.6
Xuzhou	0.35	0.49	0.16	0.47	0.35	0.74	0.47	0.65
Yangzhou	0.33	0.36	−0.05	0.41	0.33	0.54	0.24	0.55
Yinchuan	0.21	0.08	−0.9	0.94	0.21	0.1	−0.82	0.92
Zhengzhou	0.62	0.49	−0.24	0.52	0.62	0.75	0.1	0.49
Zhuhai	0.26	0.16	−0.6	0.71	0.26	0.2	−0.51	0.7

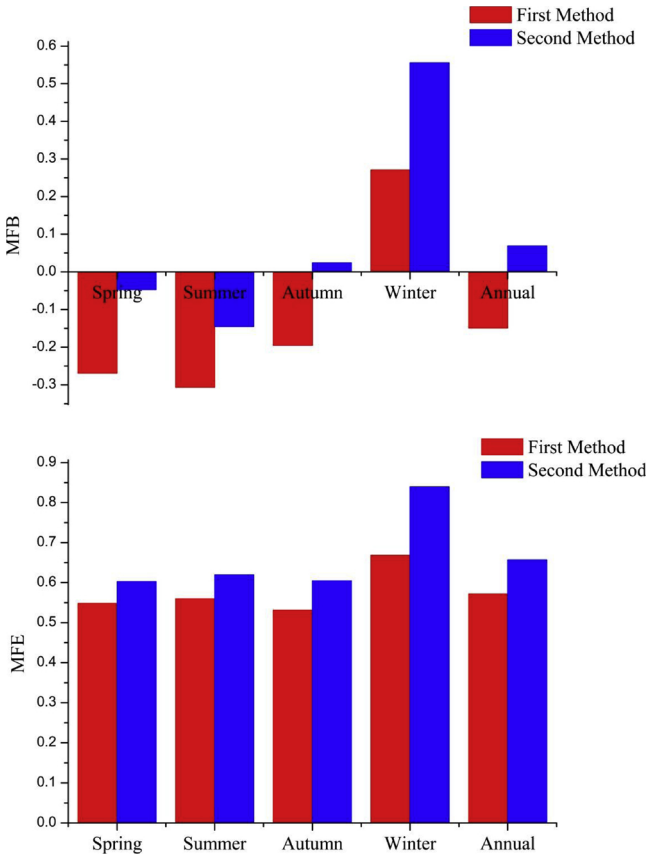

Fig. 1. MFB and MFE in different seasons with the two methods.

fractional error (MFE), mean normalized bias (MNB), and mean normalized error (MNE). Predicted O_3 generally has an MNB ≤ ± 15% and an MNE ≤ 35%, within the O_3 performance criteria suggested by the U.S. EPA (2007). Predicted $PM_{2.5}$ generally has an MFB ≤ ± 60% and an MFE ≤ 75%, meeting the $PM_{2.5}$ criteria suggested by Boylan and Russell (2006). Model predictions of $PM_{2.5}$ components were compared to observations at a few monitoring sites in different regions of China, inclding elemental carbon (EC), organic carbon (OC) (Hu et al., 2017b), sulfate, nitrate, and ammonia (Shi et al., 2017). Overall, the model captured the observed temporal and spatial variation and showed good agreement with observations at multiple sites. Model predicted source contributions to EC agreed with the source contributions estimated by a recetpor-based mehtod (Hu et al., 2015b). The evaluation exercise for the source-oriented CMAQ model builds confidence in further study to estimate the source contributions to different $PM_{2.5}$ components (Shi et al., 2017) and to visibility impairment in the current study.

2.2. Estimation of light extinction coefficient

Visual impairment in the atmosphere is caused by scattering and absorbing light by gases and particles. The attenuation of light in the atmosphere is usually quantified by light extinction coefficient (b_{ext}, km^{-1}). b_{ext} is usually decomposed into the contributions from scattering and absorption associated with gases and particles:

$$b_{ext} = b_{ag} + b_{sg} + b_{ap} + b_{sp} \quad (1)$$

where b_{ag} is the gas absorption coefficient mainly due to NO_2, b_{sg} is the Rayleigh scattering coefficient by clean air, b_{ap} is the absorption coefficient due to particles (mainly due to EC), and b_{sp} is the scattering coefficient due to particles (Seinfeld and Pandis, 1998).

Hygroscopic particle components such as sulfates and nitrates can grow into more efficient light-scattering sizes under high relative humidity conditions (Chow et al., 2002). According to relationships described by Pitchford et al. (2007), this growth is approximated by:

$$b_{sp,wet} = f(RH) \times b_{sp,dry} \quad (2)$$

where $b_{sp,wet}$ is the wet scattering coefficient, f(RH) is the growth function, and $b_{sp,dry}$ is the dry scattering coefficient measured by nephelometer at RH < 60%. The f(RH) curve from Malm et al. (2003) was used in this study. In addition, f(RH) obtained in Beijing (Yan et al., 2009) was also used to estimate b_{ext}, and more details are provided in the discussion section.

The absorption coefficient was approximated by multiplying the Interagency Monitoring of Protected Visual Environments (IMPROVE) mass extinction efficiency of 10 $m^2 g^{-1}$ to the EC concentration (Chow et al., 2010; Pitchford et al., 2007; Watson, 2002):

$$b_{ap}(km^{-1}) = 10(m^2 \cdot g^{-1}) \times [EC](\mu g \cdot m^{-3}) \times 0.001 \quad (3)$$

The absorption of NO_2 gas (b_{ag}) was estimated by using the absorption efficiency of Pitchford et al. (2007):

$$b_{ag}(km^{-1}) = 0.00033 \times [NO_2](ppb) \quad (4)$$

The Rayleigh scattering coefficient (b_{sg}) was assumed to be a constant value of 0.01 km^{-1} at sea level (Watson, 2002).

In the study, two methods were used to estimate b_{ext}. The original IMPROVE algorithm used in the first method takes the following form where the particle component concentrations are indicated in the brackets (Malm et al., 2000):

$$\begin{aligned} b_{ext} \approx\ & 0.003 \times f(RH) \times [Sulfate] + 0.003 \times f(RH) \times [Nitrate] \\ & + 0.004 \times [OM] + 0.01 \times [EC] + 0.001 \times [Fine\ Soil] \\ & + 0.0006 \times [Coarse\ Mass] + 0.01 \end{aligned} \quad (5)$$

The revised IMPROVE chemical extinction equation (Pitchford et al., 2007) used in the second method is:

$$\begin{aligned} b_{ext} \approx\ & 0.0022 \times f_s(RH) \times [Small\ Sulfate] + 0.0048 \times f_l(RH) \\ & \times [Large\ Sulfate] + 0.0024 \times f_s(RH) \times [Small\ Nitrate] + 0.0051 \times f_l(RH) \\ & \times [Large\ Nitrate] + 0.0028 \times [Small\ OM] + 0.0061 \times [Large\ OM] \\ & + 0.01 \times [EC] + 0.001 \times [Soil\ dust] + 0.0017 \times f_{ss}(RH) \times [Sea\ Salt] \\ & + 0.0006 \times [Coarse\ Mass] + Rayleigh\ Scattering(Site\ Specific) \\ & + 0.00033 \times [NO_2](ppb) \end{aligned} \quad (6)$$

where $f_l(RH)$ and $f_s(RH)$ represent the growth function for the large and small size sulfate and nitrate. The large and small sulfate indicate the formation through dry and aqueous mechanisms (John et al., 1990) and are defined by the IMPROVE equation as:

$$[Large\ Sulfate] = [Total\ Sulfate]^2/20,\ for\ [Total\ Sulfate] < 20 \mu g \cdot m^{-3} \quad (7)$$

$$[Large\ Sulfate] = [Total\ Sulfate],\ for\ [Total\ Sulfate] \geq 20 \mu g \cdot m^{-3} \quad (8)$$

$$[Small\ Sulfate] = [Total\ Sulfate] - [Large\ Sulfate] \quad (9)$$

The same method was used to separate total nitrate and organic mass (OM) concentrations into the large and small size fractions. OM was estimated by multiplying the OC concentration with 1.6, which is suitable for urban aerosol (Turpin and Lim, 2001). The soil fraction was estimated from the Fe level according to the global crustal abundance of 3.5% (Taylor and McLenna, 1985):

$$[Soil\ dust] = (1/0.035) \times [Fe] = 28.57 \times [Fe] \quad (10)$$

This calculation assumes that Fe is all from soil dust. Globally, the dust iron content accounts for 95% of the global atmospheric iron cycle, while the anthropogenic aerosol iron content accounts for only 5% of the global atmospheric iron cycle (Jickells et al., 2005; Luo et al., 2008). It should be noted that the dust concentrations could be overestimated by Eq. 10, especially in urban areas where anthropogenic contributions to Fe could be higher.

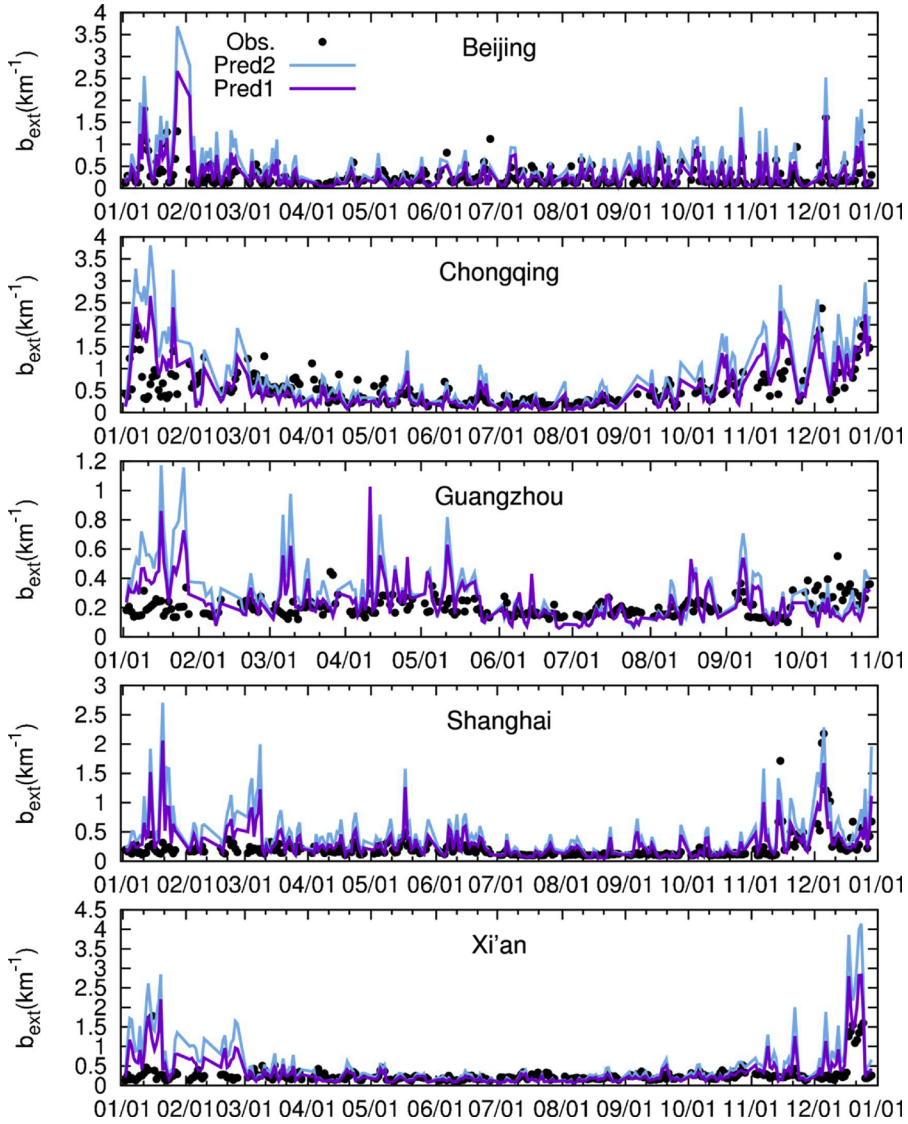

Fig. 2. Time series of observed and predicted light extinction coefficient at 5 major cities in China. Each data point in Fig. 2 represents observed daily average b_{ext} and the lines represent predicted daily average b_{ext} using the two methods.

2.3. 'Observed' b_{ext}

According to Koschmieder's formula, both the hourly visual range measurement in a one-year field observation dataset and the instantaneous visual range observation in a long-term meteorological dataset were converted to b_{ext} (Larson and Cass, 1989):

$$b_{ext} = 2.996/\text{Visual Range} \quad (11)$$

where the unit of b_{ext} is km^{-1}, and the unit of visual range is km. According to the recommendation from the WMO observation handbook, the coefficient of 2.996 is used because of the contrast threshold selection of 0.05 (WMO, 2008). The daily visual range data was downloaded from the National Climate Data Center (NCDC) (ftp://ftp.ncdc.noaa.gov/pub/data/noaa/). Quality control on the visibility data was performed following the method described by Li et al. (2016b). What about the hourly dataset?

3. Results

3.1. Model evaluation on b_{ext}

Table 1 shows the statistical performance evaluation of the predicted b_{ext} in fifty-nine cities in China. The locations of fifty-nine cities are in Fig. 3e. Mean observed values (MO), mean predicted values (MP), MFB, and MFE of predictions with the two methods were calculated. The MFB and MFE were calculated by:

$$\text{MFB} = \frac{1}{N}\sum_{i=1}^{N}\frac{(C_m - C_o)}{(C_m + C_o)/2} \quad (12)$$

$$\text{MFE} = \frac{1}{N}\sum_{i=1}^{N}\frac{|C_m - C_o|}{(C_m + C_o)/2} \quad (13)$$

where C_m is the model-estimated concentration, C_o is the observed concentration, and N equals the number of estimate–observation pairs' data.

The criteria for visibility by models recommended by Boylan and Russell (2006) are MFB within ± 0.6 and MFE less than 0.75, which are considered as acceptable model performances. In fifty out of the fifty-nine cities, the values for MFB and MFE of b_{ext} calculated using both methods comply with the performance criteria. Results from the second method are slightly better than the first method in most cities in general. The nine cities where MFB and MFE do not meet the criteria are Changsha, Lasa, Lishui, Wenzhou, Wuhan, Yinchuan, Jinhua, Lanzhou, and Quzhou with the first method, and are Changsha, Lasa, Lishui,

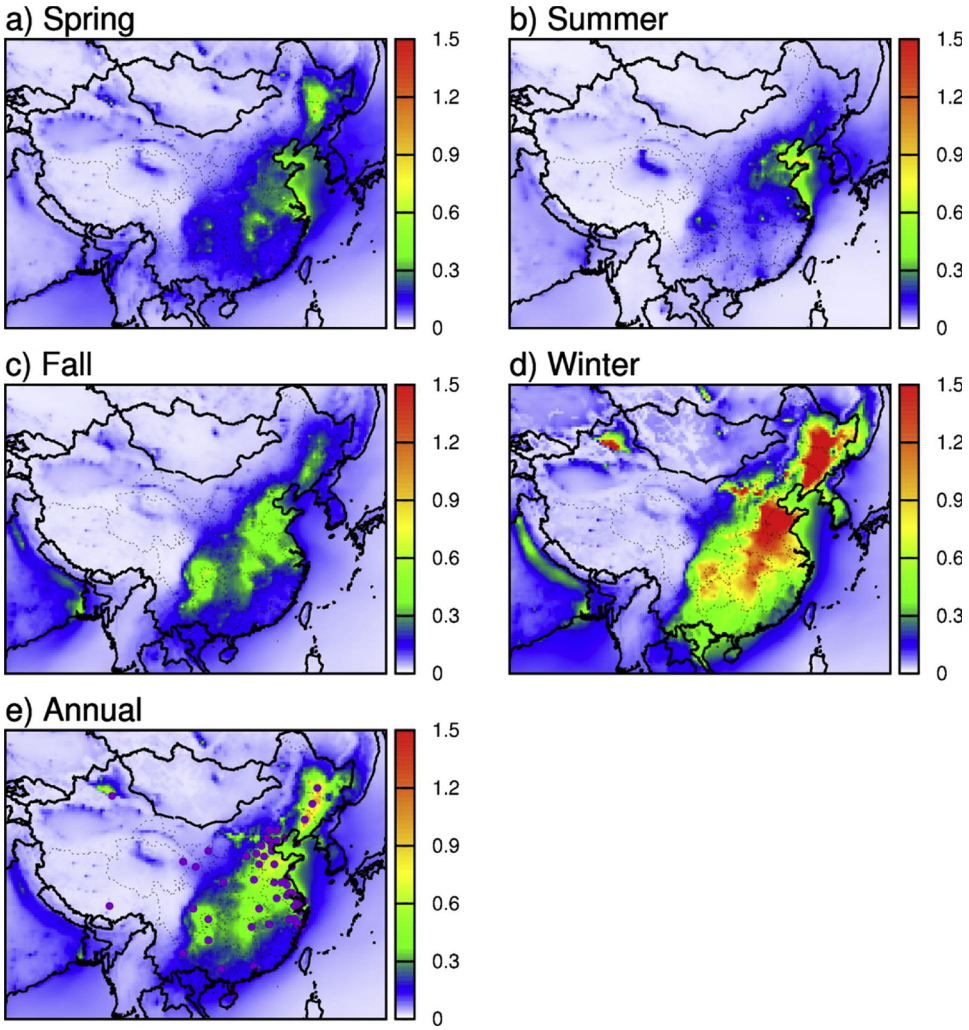

Fig. 3. Spatial distribution of seasonally- and annually-average of b_{ext}, unit is km^{-1}. The locations of fifty-nine cities are in Fig. 3e.

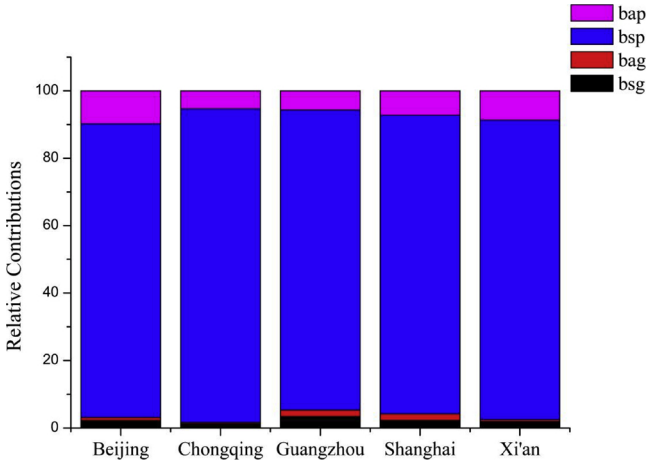

Fig. 4. The relative contributions of b_{ag}, b_{sg}, b_{ap}, and b_{sp} to the total light extinction coefficient in the 5 major cities in China. Where b_{ag} is the gas absorption coefficient, b_{sg} is the Rayleigh scattering coefficient, b_{ap} is the absorption coefficient, and b_{sp} is the scattering coefficient.

Wenzhou, Wuhan, Yinchuan, Guiyang, Haerbin, and Shenyang with the second method. Predicted $PM_{2.5}$ concentrations at these cities are largely biased from observations (Figure S1) and therefore cause the large bias in predicted b_{ext}.

Fig. 1 shows MFB and MFE in different seasons and the whole year with the two methods. Both methods yield negative MFB values in spring, summer, fall and the whole year, which means that the model underestimates the b_{ext}. This is consistent with the underprediction of $PM_{2.5}$ in spring, summer and fall, as shown in Figure S2. MFB values are positive in winter, indicating overestimates of b_{ext} by the model. In general, the MFB values, which range from -0.29 to 0.56, all meet the performance criteria; the MFE values also meet the criteria of 0.75 except in winter (MFE value of 0.84).

Fig. 2 shows time-series of daily observed and predicted b_{ext} at Beijing, Chongqing, Guangzhou, Shanghai, and Xi'an five mega-cities in China. The five cities are economic and transportation centers the North China Plain, Yangtze River Delta, Pearl River Delta, Guanzhong Plain and Sichuan Basin of China. These five regions are the most populous regions and also have been suffering from the most serious air pollution problems in China (Hu et al., 2015a). Predictions with the two methods are included in the comparison. Each data point in Fig. 2 represents observed daily average b_{ext} and the lines represent predicted daily average b_{ext} using the two methods. The daily average values of predicted b_{ext} using the two methods are generally consistent with observations in spring, summer, and fall at the five cities. The MFB values of the five cities using the first method are -0.07, -0.15, 0.07, 0.23 and 0.05, and are 0.17, 0.13, 0.19, 0.48 and 0.3 with the second method. Predicted daily-averaged b_{ext} using the two methods in winter is larger than observations at the five cities, consistent with results from Fig. 1. The second method indicates a slightly larger b_{ext} than the first method.

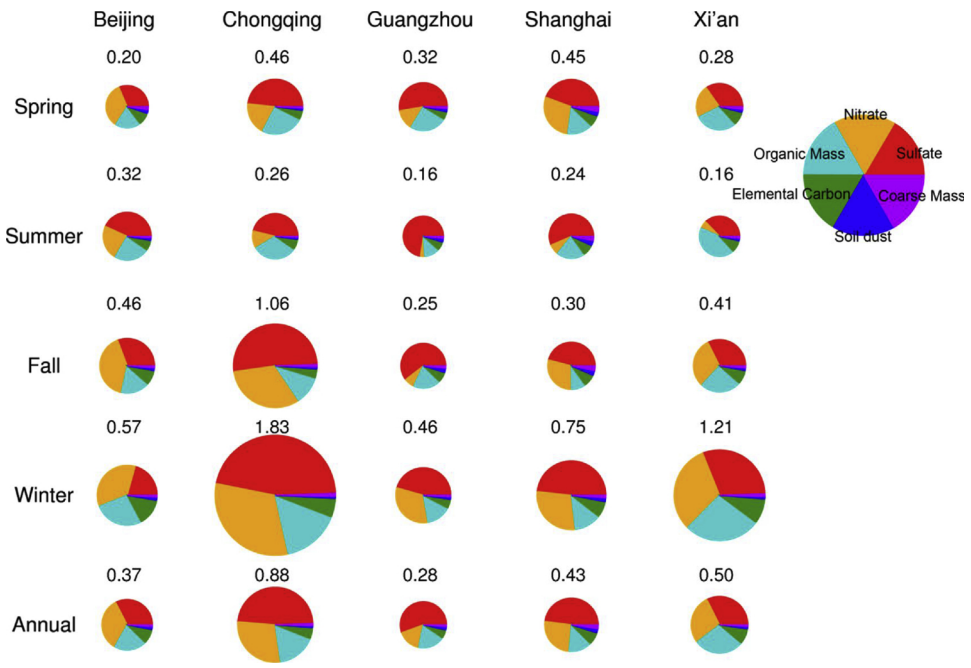

Fig. 5. Seasonally- and annually-average contributions of different particle compositions to $b_{ap}+b_{sp}$ in the 5 major cities in China. The number above each pie represents the value of $b_{ap}+b_{sp}$ in the unit of km^{-1}.

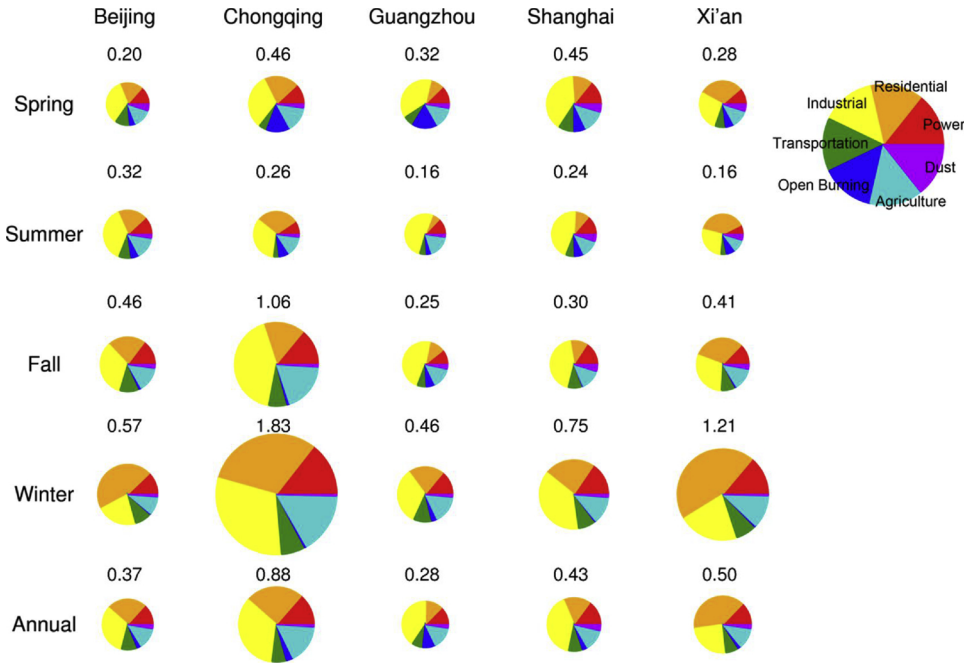

Fig. 6. Seasonally- and annually-averaged contributions of different sources to $b_{ap}+b_{sp}$ in the 5 major cities in China. The number above each pie represents $b_{ap}+b_{sp}$ in the unit of km^{-1}.

b_{ext} calculated by the second method is used in the rest of the analyses in the study.

3.2. Contributions of different components to b_{ext}

Fig. 3 shows the spatial distribution of seasonally- and annually-averaged b_{ext} in 2013. Clear seasonal and spatial variations are found in b_{ext}. In eastern China, the annual average b_{ext} is greater than 0.3 km^{-1}, larger than that in western China (< 0.1 km^{-1}), due to the influence of human activities. Moreover, the b_{ext} in winter is greater than 0.9 km^{-1} in large areas in the eastern and northeastern China. The value is several times higher than that of other seasons in the same regions. This difference is mainly attributed to more intensive emissions of air pollutants and weaker atmospheric transport and dispersion in winter.

As shown in (Eq. 1), b_{ext} is composed of four components, i.e., b_{ag}, b_{sg}, b_{ap}, and b_{sp}. Fig. 4 illustrates the relative contributions of the four components to the total b_{ext} in the five major cities shown in Fig. 2. b_{sp} has the largest relative contribution in all the five cities, around or more than 90%. b_{ap} is the second important factor, contributing to about 8% of b_{ext}. The contributions of b_{ag} and b_{sg} are very small, and mostly less than 2%. Since the effects of gaseous pollutants are negligible, only b_{ap} + b_{sp} is considered in the following b_{ext} source apportionment

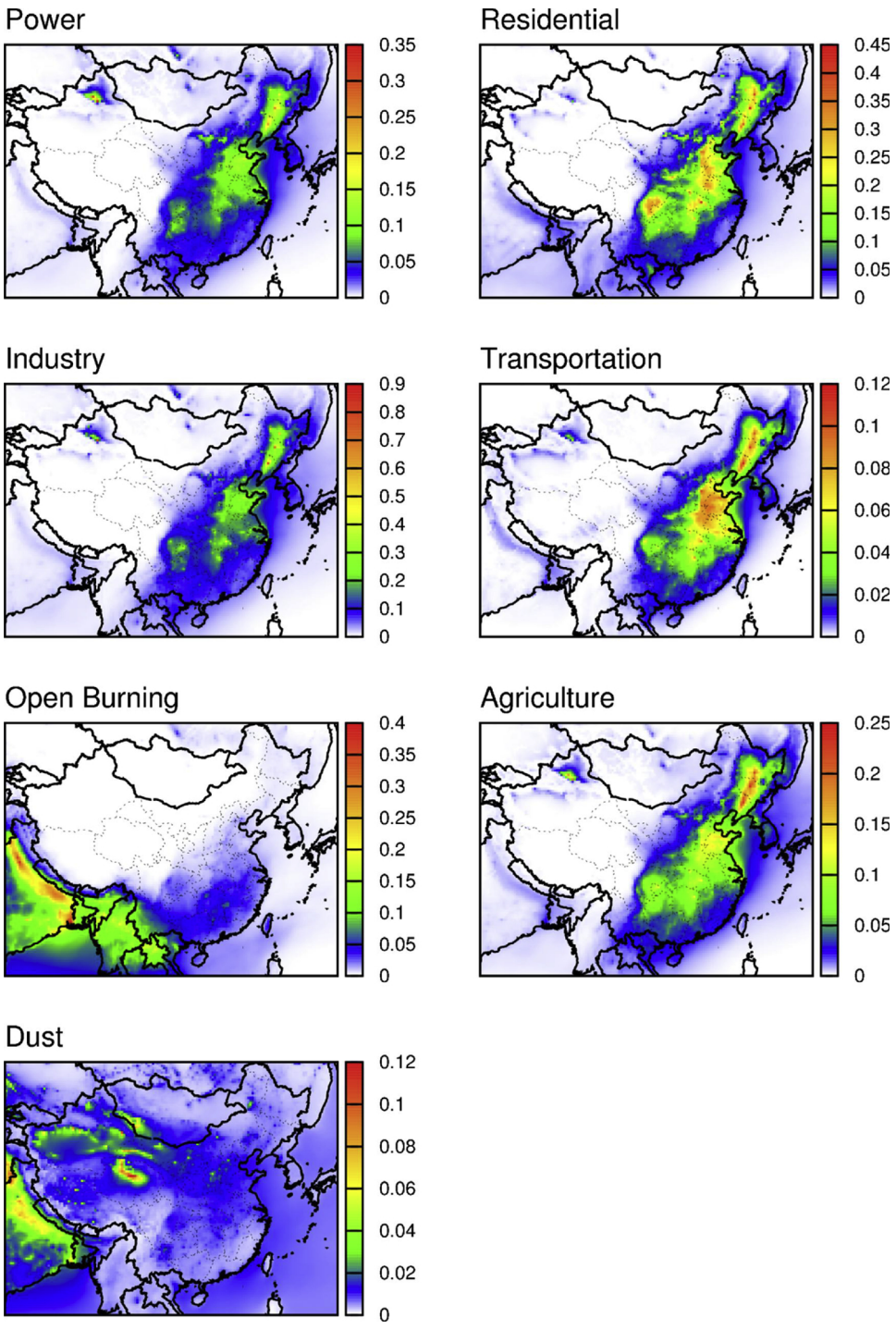

Fig. 7. Annual average regional source contributions of $b_{sp} + b_{ap}$. Unit in km^{-1}.

analyses.

Fig. 5 shows the contributions of different particle components to the seasonal and annual average of b_{ap} + b_{sp} in the five cities. The contribution of water vapor on visibility is attributed to particle components (i.e., sulfate, nitrate, sea salt, etc.) according to the f(RH) function associated with them. Except for Beijing, the b_{ap} + b_{sp} values exhibit similar seasonal variations, reaching the highest value in winter and decreasing to the lowest in summer. The lowest b_{ext} in Beijing occurs in the spring. Sulfate makes the largest annual average contribution to b_{ext} in Chongqing, Guangzhou, Shanghai, and Xi'an, accounting for 48.7%, 55.7%, 47.9% and, 32.3%, respectively. The second largest contributor is nitrate (16.1–34.2%) in Beijing, Chongqing, and Shanghai, and organic mass (14.0–28.5%) in Guangzhou and Xi'an. Elemental carbon is also important, accounting for 4.8–9.3% in the five cities. Different components have different seasonal variations. In Beijing, Guangzhou, Shanghai, and Xi'an, the contribution of sulfate in summer is larger than that in spring, fall and winter. The contribution of nitrate in summer is relatively smaller than that in spring, fall, and winter. The contribution of organic mass increases from spring to summer and from fall to winter but decreases from summer to fall in Beijing, Chongqing, Shanghai, and Xi'an. This trend is opposite in Guangzhou.

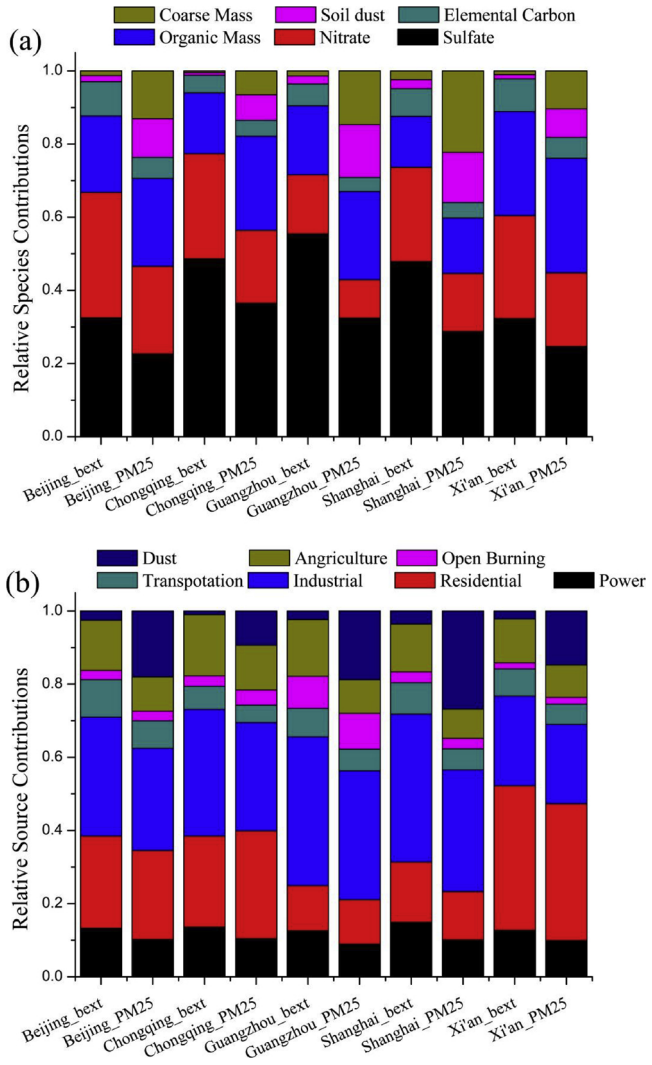

Fig. 8. Comparison of source contributions and species contributions to $PM_{2.5}$ mass and light extinction coefficient. The suffix of _PM25 is the contribution to $PM_{2.5}$ mass and the suffix of _bext is the contribution to light extinction coefficient.

3.3. Source contributions to b_{ext}

Fig. 6 shows the seasonally- and annually-averaged contributions of different sources to b_{ap} + b_{sp} in the five major cities. The source contributions to annually-averaged b_{ap} + b_{sp} are similar in Beijing, Guangzhou, Chongqing, and Shanghai. The industrial source is the dominant source, contributing 33–41% to the total. Agriculture, power, and residential source are also important, contributing 13–17%, 13–15%, and 12–25%, respectively. Source contributions exhibit clear seasonal variations. Residential emission is higher in winter, with relative contributions of approximately 45% in Beijing and Xi'an, which is about 2 times of that in Guangzhou (21%) and Shanghai (23%). In summer, the power source in Beijing, Chongqing, Shanghai and Xi'an and the transportation source in the five cities has the lowest contribution during the year. The contribution of the industrial source is larger in summer and fall than that in spring and winter in Beijing, Guangzhou, and Shanghai. Source contributions from open burning, agriculture, and dust emissions also exhibit substantial seasonal variations. Open burning in spring and summer is more important in most cities except in Guangzhou. Agriculture contributes less in summer than in the other seasons. Dust contributes less in winter than in other seasons in the five cities.

Fig. 7 shows the regional source apportionment of annually-averaged $b_{ap}+b_{sp}$. The seasonally-average results are shown in Figure S3 in the supplemental materials. Contribution from the power source sector ($> 0.1\ km^{-1}$) is higher in the North China Plain, Northeast China, and the Sichuan Basin than in other regions. The industrial sector has a similar spatial pattern as the power sector, but with a greater contribution of over $0.2\ km^{-1}$ in the North China Plain, Northeast China, and the Sichuan Basin. The residential emission sector exhibits substantial spatial variations. It is an important source contributing to b_{ap} + b_{sp}, with more than $0.1\ km^{-1}$ in spring, summer, and fall in the North China Plain, the Northeast Plain and the Sichuan Basin. Its contribution reaches more than $0.4\ km^{-1}$ in winter. The contribution of agriculture to b_{ap} + b_{sp} is higher in eastern China due to intensive agricultural activities in this region. The contribution is larger in winter due to more ammonium sulfate and ammonium nitrate formation than other seasons. Open burning is an important source in southern China in the spring. This is likely attributed to the transport of emissions from Southeast Asia countries (Chen et al., 2017). Open burning is also important in North China Plain and Sichuan basin in summer. The dust source shows important contribution in northwest China, due to a large amount of fugitive dust emission in this region. The contribution of dust is relatively small in the eastern and southern China.

4. Discussion

Fig. 8a shows the comparison of the composition contributions to $PM_{2.5}$ mass concentrations and to b_{ext}. In all the five cities, soil dust, coarse mass, and OM contribute much less to b_{ext} than that to the total $PM_{2.5}$ mass. However, sulfate, nitrate, and EC show an opposite trend. Therefore, sulfate, nitrate, and EC are more important to b_{ext}. In addition, source contributions to $PM_{2.5}$ mass are also different from those to b_{ext}, as shown in Fig. 8b. Dust source exhibits greater influence on the total $PM_{2.5}$ mass than to b_{ext}. Impacts of power, industrial and agriculture sources are stronger on b_{ext} than the total $PM_{2.5}$ mass. This trend is similar in all five cities. Sources that contribute largely to secondary inorganic components, such as power, industrial and agriculture sources, are more important to b_{ext} then to $PM_{2.5}$ mass, therefore reducing emissions from these sources will be effective for improving visibility.

The predicted values of source contributions to b_{ext} in the current study are affected by a few factors. Firstly, uncertainties in emission data affect the accuracy of the estimated source contributions to the b_{ext}. Previous studies indicated that emission estimation was affected by uncertainties associated with the emission factors and activity levels (Lei et al., 2011). In addition, the uncertainties in emissions vary in different regions of China. Estimation of the emissions in the Pearl River Delta, North China Plain, and Yangtze River Delta regions are usually more accurate, because research on air quality problems in these three regions started much earlier than other regions in China (Bouarar et al., 2019; Cheng et al., 2013a; Liu et al., 2018). As a result, source contribution predictions of b_{ext} are more accurate than other regions such as western China. Quantitative analysis of the effects of uncertainties in emissions on the source contribution estimation is highly valuable in future studies when uncertainties in emissions of each sector in the inventory become available.

Secondly, the IMPROVE and revised IMPROVE algorithms are used to calculate b_{ext} with different PM chemical compositions. These relationships were developed based on the U.S. data and are likely different in China, as indicated by previous observational studies (Cao et al., 2012b; Jung et al., 2009a, b). Table 2 shows the statistical performance evaluation of the predicted b_{ext} in fifty-nine cities in China using Beijing's growth functions, reported by Yan et al. (2009), using the revised algorithm. Two growth functions were provided by Yan et al. (2009), one is for the 'clean' conditions and the other is for the 'polluted' condition in Beijing. The two growth functions were both used to estimate b_{ext} and the results were compared to the estimations

with growth function from Malm et al. (2003). The red numbers in Table 2 indicate that the result of Beijing's data becomes worse, and the blue numbers indicate that the result becomes better. The results show that the value of twenty-nine cities under the clean condition and thirty cities under the polluted condition have improved, but the number of cities that do not meet the standards has also increased. The results in Beijing and cities in the North China Plain (the region in which Beijing is located) are all improved. But the results in some other cities, especially cities in south China become worse. The results indicate that the parameters obtained in Beijing do not apply to other regions. Developing the local relationships between b_{ext} and PM compositions in China will lower the discrepancies between the predicted and observed b_{ext} and thus improve the accuracy of estimated source contributions of b_{ext} using the source-oriented model.

The aerosol optical properties are influenced by the mixing state of PM (Curci et al., 2015). Therefore, further research is recommended to more accurately represent the aerosol mixing state in the model in order to accurately simulate the relevant optical properties. The influence of brown carbon optical properties is also important, but the relationships between the emission source and optical properties of brown carbon are not well established and need more research (Yan et al., 2018). Relatively larger discrepancies between observed and estimated b_{ext} in winter were observed and this likely causes bias in source contribution estimation. Above mentioned factors, such as uncertainties associated with emissions in winter, relationships between b_{ext} and particle compositions, model treatments in particle mixing states and brown carbon, etc., can contribute to the discrepancies. To elucidate clearly the exact contributions of the different factors to the

Table 2
Model performance of predicted light extinction coefficients in 59 cities in China using Beijing's growth functions.
XXX

City	Clean				Polluted			
	MO	MP	MFB		MO	MP	MFB	MFE
Baoding	0.29	0.46	0.11	0.57	0.29	0.48	0.15	0.58
Beijing	0.29	0.33	-0.01	0.47	0.29	0.35	0.01	0.47
Cangzhou	0.28	0.4	0.05	0.53	0.28	0.42	0.09	0.54
Changchun	0.27	0.32	-0.22	0.67	0.27	0.34	-0.18	0.67
Changsha	0.24	0.73	0.81	0.87	0.24	0.77	0.85	0.89
Chengde	0.15	0.22	0.06	0.58	0.15	0.23	0.08	0.6
Chengdu	0.3	0.48	0.31	0.53	0.3	0.51	0.34	0.54
Chongqing	0.53	0.51	-0.18	0.47	0.53	0.55	-0.13	0.46
Dalian	0.22	0.19	-0.37	0.62	0.22	0.21	-0.34	0.62
Fuzhou	0.2	0.11	-0.7	0.8	0.2	0.12	-0.66	0.78
Guangzhou	0.2	0.19	-0.18	0.51	0.2	0.21	-0.12	0.5
Guiyang	0.24	0.36	-0.03	0.66	0.24	0.39	0.03	0.67
Haerbin	0.23	0.46	0.38	0.66	0.23	0.5	0.42	0.7
Haikou	0.15	0.13	-0.47	0.73	0.15	0.13	-0.44	0.72
Handan	0.39	0.66	0.25	0.52	0.39	0.69	0.28	0.53
Hangzhou	0.55	0.37	-0.33	0.54	0.55	0.4	-0.28	0.51
Hefei	0.41	0.55	0.07	0.5	0.41	0.58	0.12	0.5
Hengshui	0.25	0.49	0.35	0.59	0.25	0.52	0.38	0.61
Huaian	0.61	0.4	-0.48	0.67	0.61	0.43	-0.43	0.64
Huhehaote	0.19	0.18	-0.27	0.66	0.19	0.19	-0.24	0.67
Huzhou	0.44	0.29	-0.48	0.62	0.44	0.32	-0.42	0.58
Jiaxing	0.27	0.28	-0.07	0.55	0.27	0.3	-0.02	0.55
Jinan	0.24	0.46	0.39	0.64	0.24	0.47	0.41	0.65
Jinhua	0.28	0.17	-0.7	0.81	0.28	0.18	-0.67	0.79
Kunming	0.19	0.18	-0.38	0.78	0.19	0.19	-0.35	0.77
Langfang	0.36	0.45	-0.03	0.54	0.36	0.47	0	0.54
Lanzhou	0.21	0.13	-0.66	0.77	0.21	0.13	-0.65	0.77
Lasa	0.1	0.02	-1.35	1.35	0.1	0.02	-1.35	1.35
Lianyungang	0.39	0.33	-0.3	0.62	0.39	0.35	-0.25	0.61
Lishui	0.3	0.13	-0.97	1.03	0.3	0.14	-0.95	1.01
Nanchang	0.32	0.29	-0.34	0.57	0.32	0.31	-0.31	0.56
Nanjing	0.37	0.42	-0.04	0.48	0.37	0.44	0	0.48
Nanning	0.21	0.23	-0.16	0.56	0.21	0.24	-0.11	0.56
Nantong	0.45	0.43	-0.12	0.49	0.45	0.46	-0.06	0.47
Qingdao	0.31	0.36	-0.06	0.57	0.31	0.38	-0.01	0.56
Qinghuang	0.23	0.36	0.11	0.6	0.23	0.38	0.16	0.62
Quzhou	0.36	0.2	-0.72	0.81	0.36	0.21	-0.69	0.79

(*continued on next page*)

Table 2 (*continued*)

XXX

Shanghai	0.23	0.31	0.2	0.48	0.23	0.32	0.24	0.49
Shaoxing	0.26	0.21	-0.43	0.64	0.26	0.22	-0.39	0.61
Shenyang	0.23	0.46	0.22	0.67	0.23	0.49	0.26	0.68
Shijiazhuang	0.32	0.45	0.01	0.57	0.32	0.47	0.04	0.58
Suqian	0.38	0.4	-0.14	0.54	0.38	0.42	-0.1	0.53
Suzhou	0.31	0.26	-0.34	0.54	0.31	0.27	-0.3	0.52
Taiyuan	0.24	0.3	0.05	0.45	0.24	0.31	0.08	0.46
Taizhoushi	0.35	0.41	0.04	0.49	0.35	0.44	0.09	0.49
Taizhou	0.3	0.25	-0.25	0.47	0.3	0.26	-0.21	0.44
Tangshan	0.3	0.44	0.22	0.5	0.3	0.47	0.26	0.52
Tianjin	0.32	0.44	0.07	0.56	0.32	0.45	0.1	0.56
Wenzhou	0.24	0.11	-0.91	0.98	0.24	0.11	-0.89	0.96
Wuhan	0.28	0.94	0.86	0.91	0.28	1.01	0.9	0.94
Wulumuqi	0.13	0.13	-0.48	0.75	0.13	0.13	-0.45	0.75
Wuxi	0.41	0.3	-0.42	0.56	0.41	0.32	-0.37	0.54
Xian	0.26	0.39	0.11	0.55	0.26	0.41	0.13	0.55
Xining	0.14	0.11	-0.46	0.66	0.14	0.11	-0.45	0.65
Xuzhou	0.35	0.54	0.22	0.58	0.35	0.57	0.25	0.58
Yangzhou	0.33	0.37	-0.07	0.51	0.33	0.39	-0.03	0.5
Yinchuan	0.21	0.09	-0.92	0.99	0.21	0.09	-0.92	0.99
Zhengzhou	0.62	0.57	-0.1	0.51	0.62	0.58	-0.08	0.5
Zhuhai	0.26	0.13	-0.81	0.88	0.26	0.14	-0.77	0.85

discrepancies, more studies with comprehensive measurements of $PM_{2.5}$ chemical, physical and optical properties are needed in the future.

5. Conclusions

In this study, a CMAQ source-oriented air quality model was used to simulate the contributions of different sources to air pollutants that affect the b_{ext} during the whole year of 2013 in China. b_{ext} was calculated using the predicted concentrations of these pollutant compositions with the IMPROVE and revised IMPROVE algorithms. The predicted b_{ext} is in general agreement with b_{ext} derived from observed visibility range in spring, summer, and fall, but is slightly over-predicted during winter of 2013. The b_{ext} is mainly affected by PM absorption (due to EC) and scattering (mainly due to sulfate, nitrate, and OM components). The source contributions to the b_{ext} and their seasonal variations in Beijing, Chongqing, Guangzhou, Shanghai, and Xi'an are similar. In Beijing, Chongqing, Guangzhou, and Shanghai, the industry sector is the largest source to b_{ext}, followed by the residential source which is very important especially in winter. The contributions of power and agriculture emissions are also important. Overall, the annual b_{ext} of 2013 in China is mainly attributed to emissions from industrial (36%), residential (20%), agricultural (15%), power plants (14%), transportation (8%), open burning (4%) and dust (3%). Source contributions to b_{ext} vary substantially in different regions. The main source sectors of the North China Plain, Northeast China, and Sichuan Basin contribute more than other regions. Control of emissions from industrial, residential and agricultural sources are recommended to improve visibility in China, with the different region- and season- specific control strategies.

Acknowledgements

This work was supported by the National Key R&D Program of China (2016YFC0203500, Task #2); the National Natural Science Foundation of China (41675125, 91544221, 41705102); Public Welfare Projects for Environmental Protection (201509001); Jiangsu Distinguished Professor Project2191071503201; Jiangsu Six Major Talent Peak Project2015-JNHB-010.

Appendix A. Supplementary data

Supplementary material related to this article can be found, in the online version, at doi:https://doi.org/10.1016/j.resconrec.2018.12.029.

References

Bouarar, I., Brasseur, G., Petersen, K., Granier, C., Fan, Q., Wang, X., Wang, L., Ji, D., Liu, Z., Xie, Y., Gao, W., Elguindi, N., 2019. Influence of anthropogenic emission inventories on simulations of air quality in China during winter and summer 2010. Atmos. Environ. 198, 236–256.

Boylan, J.W., Russell, A.G., 2006. PM and light extinction model performance metrics, goals, and criteria for three-dimensional air quality models. Atmos. Environ. 40, 4946–4959. https://doi.org/10.1016/j.atmosenv.2005.09.087.

Cao, J.-j., Wang, Q.-y., Chow, J.C., Watson, J.G., Tie, X.-x., Shen, Z.-x., Wang, P., An, Z.-s., 2012a. Impacts of aerosol compositions on visibility impairment in Xi'an, China. Atmos. Environ. 59, 559–566. https://doi.org/10.1016/j.atmosenv.2012.05.036.

Cao, J.J., Wang, Q.Y., Chow, J.C., Watson, J.G., Tie, X.X., Shen, Z.X., Wang, P., An, Z.S., 2012b. Impacts of aerosol compositions on visibility impairment in Xi'an, China. Atmos. Environ. 59, 559–566.

Chang, D., Song, Y., Liu, B., 2009. Visibility trends in six megacities in China 1973–2007. Atmos. Res. 94, 161–167. https://doi.org/10.1016/j.atmosres.2009.05.006.

Che, H.Z., Zhang, X.Y., Yang, Y., Zhou, Z.J., Qu, J.J., Hao, X.J., 2009. Haze trends over the capital cities of 31 provinces in China, 1981-2005. Theor. Appl. Climatol. 97, 235–242.

Chen, J., Ying, Q., Kleeman, M.J., 2009. Source apportionment of visual impairment during the California regional PM10/PM2.5 air quality study. Atmos. Environ. 43, 6136–6144. https://doi.org/10.1016/j.atmosenv.2009.09.010.

Chen, J., Li, C., Ristovski, Z., Milic, A., Gu, Y., Islam, M.S., Wang, S., Hao, J., Zhang, H., He, C., Guo, H., Fu, H., Miljevic, B., Morawska, L., Thai, P., Lam, Y.F., Pereira, G., Ding, A., Huang, X., Dumka, U.C., 2017. A review of biomass burning: emissions and impacts on air quality, health and climate in China. Sci. Total Environ. 579, 1000–1034.

Chen, K., Guo, H., Hu, J., Kota, S., Deng, W., Ying, Q., Myllyvirta, L., Dahiya, S., Zhang, H., 2019. Projected air quality and health benefits from future policy interventions in

India. Resour. Conserv. Recycl. 142, 232–244. https://doi.org/10.1016/j.resconrec.2018.12.008.
Cheng, Z., Wang, S., Jiang, J., Fu, Q., Chen, C., Xu, B., Yu, J., Fu, X., Hao, J., 2013a. Long-term trend of haze pollution and impact of particulate matter in the Yangtze River Delta, China. Environ. Pollut. 182, 101–110. https://doi.org/10.1016/j.envpol.2013.06.043.
Cheng, Z., Wang, S.X., Jiang, J.K., Fu, Q.Y., Chen, C.H., Xu, B.Y., Yu, J.Q., Fu, X., Hao, J.M., 2013b. Long-term trend of haze pollution and impact of particulate matter in the Yangtze River Delta, China. Environ. Pollut. 182, 101–110. https://doi.org/10.1016/j.envpol.2013.06.043.
Chow, J.C., Bachmann, J.D., Wierman, S.S.G., Mathai, C.V., Malm, W.C., White, W.H., Mueller, P.K., Kumar, N., Watson, J.G., 2002. Visibility: science and regulation. J. Air Waste Manage. Assoc. 52, 973–999. https://doi.org/10.1080/10473289.2002.10470844.
Chow, J.C., Watson, J.G., Green, M.C., Frank, N.H., 2010. Filter light attenuation as a surrogate for elemental carbon. J. Air Waste Manage. Assoc. 60, 1365–1375. https://doi.org/10.3155/1047-3289.60.11.1365.
Curci, G., Hogrefe, C., Bianconi, R., Im, U., Balzarini, A., Baró, R., Brunner, D., Forkel, R., Giordano, L., Hirtl, M., Honzak, L., Jiménez-Guerrero, P., Knote, C., Langer, M., Makar, P.A., Pirovano, G., Pérez, J.L., San José, R., Syrakov, D., Tuccella, P., Werhahn, J., Wolke, R., Žabkar, R., Zhang, J., Galmarini, S., 2015. Uncertainties of simulated aerosol optical properties induced by assumptions on aerosol physical and chemical properties: an AQMEII-2 perspective. Atmos. Environ. 115, 541–552.
Deng, J., Wang, T., Jiang, Z., Xie, M., Zhang, R., Huang, X., Zhu, J., 2011. Characterization of visibility and its affecting factors over Nanjing, China. Atmos. Res. 101, 681–691.
Deng, J.J., Xing, Z.Y., Zhuang, B.L., Du, K., 2014. Comparative study on long-term visibility trend and its affecting factors on both sides of the Taiwan Strait. Atmos. Res. 143, 266–278. https://doi.org/10.1016/j.atmosres.2014.02.018.
Hu, J., Qi, Y., Wang, Y., Zhang, H., 2015a. Characterizing multi-pollutant air pollution in China: comparison of three air quality indices. Environ. Int. 84, 17.
Hu, J., Wu, L., Zheng, B., Zhang, Q., He, K., Chang, Q., Li, X., Yang, F., Ying, Q., Zhang, H., 2015b. Source contributions and regional transport of primary particulate matter in China. Environ. Pollut. 207, 31–42.
Hu, J., Chen, J., Ying, Q., Zhang, H., 2016. One-year simulation of ozone and particulate matter in China using WRF/CMAQ modeling system. Atmos. Chem. Phys. 16, 10333–10350.
Hu, J., Huang, L., Chen, M., He, G., Zhang, H., 2017a. Impacts of power generation on air quality in China—part II: future scenarios. Resour. Conserv. Recycl. 121, 115–127. https://doi.org/10.1016/j.resconrec.2016.04.011.
Hu, J., Wang, P., Ying, Q., Zhang, H., Chen, J., Ge, X., Li, X., Jiang, J., Wang, S., Zhang, J., Zhao, Y., Zhang, Y., 2017b. Modeling biogenic and anthropogenic secondary organic aerosol in China. Atmos. Chem. Phys. 17, 77–92. https://doi.org/10.5194/acp-17-77-2017.
Hu, Y., Yao, L., Cheng, Z., Wang, Y., 2017c. Long-term atmospheric visibility trends in megacities of China, India and the United States. Environ. Res. 159, 466–473. https://doi.org/10.1016/j.envres.2017.08.018.
Huang, R.J., Zhang, Y.L., Bozzetti, C., Ho, K.F., Cao, J.J., Han, Y.M., Daellenbach, K.R., Slowik, J.G., Platt, S.M., Canonaco, F., Zotter, P., Wolf, R., Pieber, S.M., Bruns, E.A., Crippa, M., Ciarelli, G., Piazzalunga, A., Schwikowski, M., Abbaszade, G., Schnelle-Kreis, J., Zimmermann, R., An, Z.S., Szidat, S., Baltensperger, U., El Haddad, I., Prevot, A.S.H., 2014. High secondary aerosol contribution to particulate pollution during haze events in China. Nature 514, 218–222. https://doi.org/10.1038/nature13774.
Huang, L., Hu, J., Chen, M., Zhang, H., 2017. Impacts of power generation on air quality in China—part I: an overview, Resources. Conserv. Recycl. 121, 103–114. https://doi.org/10.1016/j.resconrec.2016.04.010.
Hyslop, N.P., 2009. Impaired visibility: the air pollution people see. Atmos. Environ. 43, 182–195. https://doi.org/10.1016/j.atmosenv.2008.09.067.
Jickells, T.D., An, Z.S., Andersen, K.K., Baker, A.R., Bergametti, G., Brooks, N., Cao, J.J., Boyd, P.W., Duce, R.A., Hunter, K.A., Kawahata, H., Kubilay, N., laRoche, J., Liss, P.S., Mahowald, N., Prospero, J.M., Ridgwell, A.J., Tegen, I., Torres, R., 2005. Global iron connections between desert dust, ocean biogeochemistry, and climate. Science 308, 67–71.
John, W., Wall, S.M., Ondo, J.L., Winklmayr, W., 1990. Modes in the size distributions of atmospheric inorganic aerosol. Atmos. Environ. Part A: Gen. Top. 24, 2349–2359.
Jung, J., Lee, H., Kim, Y.J., Liu, X.G., Zhang, Y.H., Gu, J.W., Fan, S.J., 2009a. Aerosol chemistry and the effect of aerosol water content on visibility impairment and radiative forcing in Guangzhou during the 2006 Pearl River Delta campaign. J. Environ. Manage. 90, 3231–3244.
Jung, J., Lee, H., Kim, Y.J., Liu, X.G., Zhang, Y.H., Hu, M., Sugimoto, N., 2009b. Optical properties of atmospheric aerosols obtained by in situ and remote measurements during 2006 Campaign of Air Quality Research in Beijing (CAREBeijing-2006). J. Geophys. Res. Atmos. 114.
Kurokawa, J., Ohara, T., Morikawa, T., Hanayama, S., Janssens-Maenhout, G., Fukui, T., Kawashima, K., Akimoto, H., 2013. Emissions of air pollutants and greenhouse gases over Asian regions during 2000–2008: Regional Emission inventory in ASia (REAS) version 2. Atmos. Chem. Phys. 13, 11019–11058. https://doi.org/10.5194/acp-13-11019-2013.
Larson, S.M., Cass, G.R., 1989. Characteristics of summer midday low-visibility events in the Los Angeles area. Environ. Sci. Technol. 23, 281–289. https://doi.org/10.1021/es00180a003.
Lei, Y., Zhang, Q., He, K.B., Streets, D.G., 2011. Primary anthropogenic aerosol emission trends for China, 1990-2005. Atmos. Chem. Phys. 11, 931–954. https://doi.org/10.5194/acp-11-931-2011.
Li, C., Martin, R.V., Boys, B.L., van Donkelaar, A., Ruzzante, S., 2016a. Evaluation and application of multi-decadal visibility data for trend analysis of atmospheric haze. Atmos. Chem. Phys. 16, 2435–2457. https://doi.org/10.5194/acp-16-2435-2016.
Li, J., Li, C.C., Zhao, C.S., Su, T.N., 2016b. Changes in surface aerosol extinction trends over China during 1980-2013 inferred from quality-controlled visibility data. Geophys. Res. Lett. 43, 8713–8719.
Liu, H., Wu, B., Liu, S., Shao, P., Liu, X., Zhu, C., Wang, Y., Wu, Y., Xue, Y., Gao, J., Hao, Y., Tian, H., 2018. A regional high-resolution emission inventory of primary air pollutants in 2012 for Beijing and the surrounding five provinces of North China. Atmos. Environ. 181, 20–33.
Luo, C., Mahowald, N., Bond, T., Chuang, P.Y., Artaxo, P., Siefert, R., Chen, Y., Schauer, J., 2008. Combustion iron distribution and deposition. Global. Biogeochem. Cycles 22.
Malm, W.C., PitchFord, M.L., Scuggs, M., Sisler, J.F., Ames, R., Copeland, S., Gebhart, K.A., Day, D.E., 2000. Spatial and Seasonal Patterns and Temporal Variability of Haze and Its Constituents in the United States, Report III. Cooperative Institute for Research in the Atmosphere.
Malm, W.C., Day, D.E., Kreidenweis, S.M., Collett, J.L., Lee, T., 2003. Humidity-dependent optical properties of fine particles during the Big Bend Regional Aerosol and Visibility Observational Study. J. Geophys. Res. Atmos. 108, 4279.
Pitchford, M., Malm, W., Schichtel, B., Kumar, N., Lowenthal, D., Hand, J., 2007. Revised algorithm for estimating light extinction from IMPROVE particle speciation data. J. Air Waste Manage. Assoc. 57, 1326–1336. https://doi.org/10.3155/1047-3289.57.11.1326.
Seinfeld, J.H., Pandis, S.N., 1998. Atmospheric Chemistry and Physics: From Air Pollution to Climate Change. Wiley Interscience.
Shi, Z., Li, J., Huang, L., Wang, P., Wu, L., Ying, Q., Zhang, H., Lu, L., Liu, X., Liao, H., Hu, J., 2017. Source apportionment of fine particulate matter in China in 2013 using a source-oriented chemical transport model. Sci. Total Environ. 601, 1476–1487. https://doi.org/10.1016/j.scitotenv.2017.06.019.
Sisler, J.F., Malm, W.C., 1994. The relative importance of soluble aerosols to spatial and seasonal trends of impaired visibility in the United States. Atmos. Environ. 28, 851–862. https://doi.org/10.1016/1352-2310(94)90244-5.
Tao, J., Zhang, L., Cao, J., Hsu, S.-C., Xia, X., Zhang, Z., Lin, Z., Cheng, T., Zhang, R., 2014. Characterization and source apportionment of aerosol light extinction in Chengdu, southwest China. Atmos. Environ. 95, 552–562. https://doi.org/10.1016/j.atmosenv.2014.07.017.
Taylor, S.R., McLenna, S.M., 1985. The Continental Crust: Its Composition and Evolution. Blackwell 315 pp.
Trijonis, J., 1984. Effect of diesel vehicles on visibility in California. Science of The Total Environment 36, 131–140. https://doi.org/10.1016/0048-9697(84)90257-2.
Turpin, B., Lim, H.J., 2001. Species contributions to PM2.5 mass concentrations: revisiting common assumptions for estimating organic mass. Aerosol Sci. Technol. 35, 602–610.
U.S. EPA, 2007. In: Agency, U. S. E. P (Ed.), Guidance on the Use of Models and Other Analyses for Demonstrating Attainment of Air Quality Goals for Ozone, PM2.5 and Regional Haze. Research Triangle Park, North Carolina.
Wang, Q.Y., Cao, J.J., Tao, J., Li, N., Su, X.O., Chen, L.W.A., Wang, P., Shen, Z.X., Liu, S.X., Dai, W.T., 2013. Long-term trends in visibility and at Chengdu, China. PLoS One 8, 68894. https://doi.org/10.1371/journal.pone.0068894.
Wang, P., Ying, Q., Zhang, H., Hu, J., Lin, Y., Mao, H., 2018. Source apportionment of secondary organic aerosol in China using a regional source-oriented chemical transport model and two emission inventories. Environ. Pollut. 237, 756–776.
Watson, J.G., 2002. Visibility: science and regulation. J. Air Waste Manage. Assoc. 52, 628–713.
WMO, 2008. Aerodrome Reports and Forecasts: a User's Handbook to the Codes. World Meteorological Organization.
Xiao, Z.M., Zhang, Y.F., Hong, S.M., Bi, X.H., Jiao, L., Feng, Y.C., Wang, Y., 2011. Q.: estimation of the main factors influencing haze, based on a long-term monitoring campaign in Hangzhou, China. Aerosol Air Qual. Res. 11, 873–882.
Yan, P., Pan, X., Tang, J., Zhou, X., Zhang, R., Zeng, L., 2009. Hygroscopic growth of aerosol scattering coefficient: a comparative analysis between urban and suburban sites at winter in Beijing. Particuology 7, 52–60. https://doi.org/10.1016/j.partic.2008.11.009.
Yan, J., Wang, X., Gong, P., Wang, C., Cong, Z., 2018. Review of brown carbon aerosols: recent progress and perspectives. Sci. Total Environ. 634, 1475–1485. http://ssl1230a75e822c6f3334851117f8769a30e1c.vpn.nuist.edu.cn/10.1016/j.scitotenv.2018.04.083.
Ying, Q., Mysliwiec, M., Kleeman, M., 2004. J.: source apportionment of visibility impairment using a three-dimensional source-oriented air quality model. Environ. Sci. Technol. 38, 1089–1101. https://doi.org/10.1021/es0349305.
Ying, Q., Feng, M., Song, D., Wu, L., Hu, J., Zhang, H., Kleeman, M.J., Li, X., 2018. Improve regional distribution and source apportionment of PM2.5 trace elements in China using inventory-observation constrained emission factors. Sci. Total Environ. 624, 355–365. https://doi.org/10.1016/j.scitotenv.2017.12.138.
Zeng, B., Wu, T., Guo, X., 2019. Interprovincial trade, economic development and the impact on air quality in China. Resour. Conserv. Recycl. 142, 204–214. https://doi.org/10.1016/j.resconrec.2018.12.002.